Composite Structures 93 (2011) 1201–1216

Contents lists available at ScienceDirect

Composite Structures

journal homepage: www.elsevier.com/locate/compstruct

Transient dynamic analysis of higher order sandwich and composite arches

Sudhakar R. Marur [a,*], Tarun Kant [b]

[a] CSS Foundation, 313, A4 Wing, Cauvery Block, NGH Complex, Koramangala, Bangalore 560 047, India
[b] Department of Civil Engineering, Indian Institute of Technology, Powai, Mumbai 400 076, India

ARTICLE INFO

Article history:
Available online 4 December 2010

Keywords:
Transient dynamics
Sandwich
Composite
Laminated arch
Curved beam
Higher order theory

ABSTRACT

A higher order refined model with isoparametric elements is proposed to study the transient dynamic response of laminated arches/curved beams. The strain field is modeled through cubic axial, cubic transverse shear and linear transverse normal strain components. As the cross-sectional warping is accurately modeled by this theory, the shear correction factor is rendered redundant. The stress–strain relationship is derived from an orthotropic lamina in a three-dimensional state of stress, so that angle-ply laminates can be studied through one-dimensional elements. Consistent mass matrix is constituted for the equation of motion, which is solved by Newmark integration scheme. The higher order formulation is validated with available results and subsequently applied to arches with various curvatures, aspect ratios, boundary conditions, loadings and lamination schemes to evaluate its transient dynamic performance and suitable conclusions are drawn.

1. Introduction

Evaluation of response of laminated arches or curved beams to transient dynamic loads is the key to the design of components, subsystems or even systems with such materials in aero space, healthcare, automotive and transportation segments due to their high strength to weight ratio. That would be feasible through the development of a suitable numerical model and that is primary focus of this paper.

Wu and Witmer studied the nonlinear transient response of an impulsively loaded ring through the displacement finite elements based on principle of virtual work [1] and developed the equation of motion for beams and rings [2] with material and geometric nonlinearities based on Euler–Bernoulli and Timoshenko [3] theories of deformation using virtual work and D'Alembert's principle. Tene et al. [4] studied plane curved beam with shear deformation and rotary inertia, subjected to static and dynamic loads through Houbolt's method and finite difference scheme. Sagartz [5] evaluated the transient response of a three-layer ring through a computational model along with an experimental study. Remseth [6] studied the nonlinear dynamic analysis of space frames, wherein curved beams were modeled through the introduction of initial deflections in the element stiffness relations.

Sheinman [7] reported an arbitrary plane curved beam with geometric nonlinearity, shear deformation, rotary inertia, initial imperfections and viscous damping, subjected to dynamic loads through Houbolt's method. Noor and Knight [8] developed a computational procedure for predicting the dynamic response of curved beam with geometric nonlinearity. Using a mixed formulation and explicit central difference method, they analyzed arches with transverse shear and rotary inertia. Noor and Peters [9] presented a large rotation dynamic analysis of curved beams with the effects of transverse shear deformation using Newmark's integration. Henrych [10] dealt with the subject of linear free and forced oscillations of planar arches and frames, with various cross-sections, rotatory and tangential inertia, transverse shear and extensionality of the neutral axis.

Hsiao and Hsiao [11] published a co-rotational finite element formulation for the dynamic analysis of a planar curved beam, based on the Euler–Bernoulli theory, wherein the nonlinear dynamic equilibrium equations are solved through Newmark integration scheme and Newton–Raphson technique. Khdeir and Reddy [12] studied the dynamic response of slightly curved cross-ply laminated composite beams to general forcing functions and for arbitrary end conditions through a model based on shallow shell theory for thin to thick arches. Huang et al. [13] analyzed the transient response of arches with variable curvature, shear deformation, rotary inertia and damping by combining the dynamic stiffness method with the Laplace transform. Gordon and Hollkamp [14] adopted implicit condensation and expansion method to predict the response of a thin, curved aluminum beam to random distributed loading.

As one can observe from the reported literature that the formulations based on classical Euler–Bernoulli theory can handle only thin sections with higher aspect ratios. While the studies based on first order theory can model deeper sections, they have

* Corresponding author.
E-mail addresses: srmarur@iitbombay.org (S.R. Marur), tkant@civil.iitb.ac.in (T. Kant).

0263-8223/$ - see front matter © 2010 Elsevier Ltd. All rights reserved.
doi:10.1016/j.compstruct.2010.11.004

Nomenclature

S	arclength of the arch
t	thickness of cross-section
R	radius of curvature
S/t	aspect ratio
$\beta(=S/R)$	subtended angle of an arch
BC	boundary condition
HOAM	higher order arch model
FOST	first order shear deformation theory of Timoshenko [3]
k	shear correction factor (5/6) for FOST
t_f	time at which the external force vector reaches zero magnitude
t_p	time at which the external force vector reaches peak value

limitations such as the need for a shear correction factor [3] and the inability to capture the cross-sectional warping – a key factor for sandwich constructions with stiff facings and weak cores. Besides, this theory cannot model the variation of transverse displacement across the thickness i.e. the transverse normal strain. Hence, there is a need for a numerical model that can accurately model and analyze deep laminated arches or curved beams. This paper aims to propose a higher order model, fulfilling that need.

This higher order theory models the cross-sectional warping through a cubic axial strain; considers the variation of transverse displacement across the thickness through a linearly varying transverse normal strain; incorporates transverse shear strain, varying cubically across the cross-section and does not require any shear correction factor and is built through standard isoparametric elements. Its elasticity matrix had been derived from an orthotropic lamina assumed to be in a three-dimensional state of stress, in such a way that even angle-ply laminations can be studied using one-dimensional elements. The equation of motion assembled through consistent mass matrix is solved by the Newmark time integration scheme.

Through the transient dynamic analyses of shallow to deep and thin to thick laminated arches with various boundary and loading conditions, the proposed higher order formulation is first validated and subsequently evaluated in a comparative manner with the first order model.

2. Theoretical formulation

The higher order arch model (HOAM), based on Taylor's series expansion [15], can be expressed, for an arch, as follows:

$$u = u_0 + z\theta_x + z^2 u_0^* + z^3 \theta_x^* \tag{1}$$

$$w = w_0 + z\theta_z + z^2 w_0^* \tag{2}$$

where z is the distance from the neutral axis to any point of interest along the depth of the arch, u_0 and w_0 are axial and transverse displacements in x–z plane, θ_x is the face rotation about y-axis (Fig. 1) and u_0^*, θ_x^*, θ_z, w_0^* are the higher order terms arising out of Taylor's series expansion and defined at the neutral axis.

The Lagrangian function is be given as

$$L = T - (U - W) \tag{3}$$

where T is the kinetic energy, U is the internal strain energy and W is the work done by the external forces/loads. The same can be expressed as

$$L = \frac{1}{2}\int \underset{\sim}{\dot{u}}^t \rho \underset{\sim}{\dot{u}}\, dv - \left\{\frac{1}{2}\int \varepsilon^t \sigma\, dv - b\int \underset{\sim}{u}^t \underset{\sim}{p}\, dx\right\} \tag{4}$$

where

$$\underset{\sim}{u} = [u\ w]^t, \quad \underset{\sim}{\dot{u}} = [\dot{u}\ \dot{w}]^t, \quad \varepsilon = [\varepsilon_x\ \varepsilon_z\ \gamma_{xz}]^t,$$
$$\sigma = [\sigma_x\ \sigma_z\ \tau_{xz}]^t, \quad \underset{\sim}{p} = [p_x\ p_z]^t \tag{4a}$$

The field variables can be expressed in terms of nodal degrees of freedom as

$$\underset{\sim}{u} = Z_d d \tag{5}$$

where

$$d = \left[u_0\ w_0\ \theta_x\ u_0^*\ \theta_x^*\ \theta_z\ w_0^*\right]^t \tag{5a}$$

$$Z_d = \begin{bmatrix} 1 & 0 & z & z^2 & z^3 & 0 & 0 \\ 0 & 1 & 0 & 0 & 0 & z & z^2 \end{bmatrix} \tag{5b}$$

The strain field for an arch [16] can be expressed as

$$\varepsilon_x = \frac{1}{(1+z/R)}(u_{,x} + w/R) \tag{6a}$$

$$\varepsilon_z = w_{,z} \tag{6b}$$

$$\gamma_{xz} = w_{,x} + u_{,z} - u/R \tag{6c}$$

where R is the radius of curvature.

Applying the displacement field from Eqs. (1) and (2) in the above equations, one gets,

$$\varepsilon_x = \varepsilon_{x0} + z^2\varepsilon_{x0}^* + z\kappa_x + z^3\kappa_x^* \tag{7a}$$

$$\varepsilon_z = \varepsilon_{z0} + z\kappa_z \tag{7b}$$

$$\gamma_{xz} = \varphi + z^2\varphi^* + z\chi_{xz} + z^3\chi_{xz}^* \tag{7c}$$

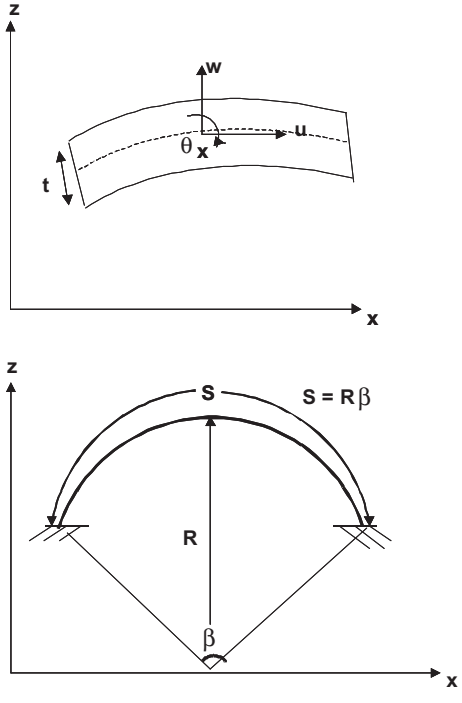

Fig. 1. Arch geometry with displacement components.

and can be expressed in matrix form as

$$\varepsilon_x = Z_a^t \varepsilon_a + Z_b^t \varepsilon_b \tag{8}$$

$$\varepsilon_z = Z_t^t \varepsilon_t \tag{9}$$

$$\gamma_{xz} = Z_s^t \gamma_s \tag{10}$$

where

$$\varepsilon_a = \left[\varepsilon_{x0}\ \varepsilon_{x0}^*\right]^t = \left[(u_{0,x} + w_0/R)\left(u_{0,x}^* + w_0^*/R\right)\right]^t \tag{11a}$$

$$\varepsilon_b = \left[\kappa_x\ \kappa_x^*\right]^t = \left[(\theta_{x,x} + \theta_z/R)\left(\theta_{x,x}^*\right)\right]^t \tag{11b}$$

$$\varepsilon_t = \left[\varepsilon_{z0}\ \kappa_z\right]^t = \left[\theta_z\ 2w_0^*\right]^t \tag{11c}$$

$$\gamma_s = \left[\varphi\ \varphi^*\ \chi_{xz}\ \chi_{xz}^*\right]^t = \left[(w_{0,x} + \theta_x - u_0/R)\left(w_{0,x}^* + 3\theta_x^* - u_0^*/R\right)\quad (\theta_{z,x} + 2u_0^* - \theta_x/R)\ (-\theta_x^*/R)\right]^t \tag{11d}$$

$$Z_a = \left[\frac{1}{(1+z/R)}\ \frac{z^2}{(1+z/R)}\right]^t \tag{11e}$$

$$Z_b = \left[\frac{z}{(1+z/R)}\ \frac{z^3}{(1+z/R)}\right]^t \tag{11f}$$

$$Z_t = [1\ z]^t \tag{11g}$$

$$Z_s = [1\ z^2\ z\ z^3]^t \tag{11h}$$

The strains of Eqs. (8)–(10) can be rewritten in a combined matrix form as

$$\varepsilon = \overline{Z}\bar{\varepsilon} \tag{12}$$

where

$$\overline{Z} = \begin{bmatrix} Z_a^t & Z_b^t & 0 & 0 \\ 0 & 0 & Z_t^t & 0 \\ 0 & 0 & 0 & Z_s^t \end{bmatrix} \tag{12a}$$

$$\bar{\varepsilon} = [\varepsilon_a\ \varepsilon_b\ \varepsilon_t\ \gamma_s]^t \tag{12b}$$

The stress–strain relationship of an orthotropic lamina in a three dimensional state of stress can be expressed as [17],

$$\sigma^o = Q\varepsilon^o \tag{13}$$

where

$$\sigma^o = [\sigma_x\ \sigma_y\ \sigma_z\ \tau_{xy}\ \tau_{yz}\ \tau_{xz}]^t \tag{13a}$$

$$\varepsilon^o = [\varepsilon_x\ \varepsilon_y\ \varepsilon_z\ \gamma_{xy}\ \gamma_{yz}\ \gamma_{xz}]^t \tag{13b}$$

and Q is given by Eqs. (A17)–(A29), in Appendix A.

By setting σ_y, τ_{xy}, τ_{yz} equal to zero in Eq. (13) and deriving the remaining stress components from the same equation, one gets the stress–strain relationship as [18],

$$\sigma = C\varepsilon \tag{14}$$

where

$$\sigma = [\sigma_x\ \sigma_z\ \tau_{xz}]^t \tag{14a}$$

$$C = \begin{bmatrix} C_{11} & C_{12} & 0 \\ C_{21} & C_{22} & 0 \\ 0 & 0 & C_{33} \end{bmatrix} \tag{14b}$$

and the expressions for various C matrix elements are given by Eqs. (B1)–(B6), in Appendix B.

The internal strain energy can be evaluated using Eqs. (12) and (14) as

$$U = \frac{1}{2}\int \varepsilon^t \sigma\, d\nu = \frac{1}{2}\int \bar{\varepsilon}^t \overline{D}\,\bar{\varepsilon}\, dx \tag{15}$$

where

$$\overline{D} = b\int \overline{Z}^t C \overline{Z}\, dz \tag{15a}$$

$$= b\int \begin{bmatrix} Z_a C_{11} Z_a^t & Z_a C_{11} Z_b^t & Z_a C_{12} Z_t^t & 0 \\ Z_b C_{11} Z_a^t & Z_b C_{11} Z_b^t & Z_b C_{12} Z_t^t & 0 \\ Z_t C_{21} Z_a^t & Z_t C_{21} Z_b^t & Z_t C_{22} Z_t^t & 0 \\ 0 & 0 & 0 & Z_s C_{33} Z_s^t \end{bmatrix} dz \tag{15b}$$

$$= \begin{bmatrix} D_{aa} & D_{ab} & D_{at} & 0 \\ D_{ba} & D_{bb} & D_{bt} & 0 \\ D_{ta} & D_{tb} & D_{tt} & 0 \\ 0 & 0 & 0 & D_{ss} \end{bmatrix} \tag{15c}$$

and the expansions of various D matrices are given by Eqs. (C3)–(C13), in Appendix C.

The kinetic energy can be expressed using Eq. (5) as

$$T = \frac{1}{2}\int (\dot{d}^t \bar{m} \dot{d})\, dx \tag{16}$$

where

$$\bar{m} = b\sum_{l=1}^{NL}\int (z_d^t \rho_l z_d)\, dz \tag{17}$$

where ρ_l is the mass density of a layer and $\bar{m}$ is given by Eq. (C12), in Appendix C.

The external work done of Eqs. (3) and (4) can be modified with Eq. (5) as

$$W = d^t \int \underset{\sim}{P}\, dx \tag{18}$$

where

$$\underset{\sim}{P} = b Z_d^t \underset{\sim}{p} \tag{18a}$$

$$= b[p_x\ p_z\ zp_x\ z^2 p_x\ z^3 p_x\ zp_z\ z^2 p_z]^t \tag{18b}$$

which can expressed as

$$\underset{\sim}{P} = [p_{x0}\ p_{z0}\ m_{x0}\ p_{x0}^*\ m_{x0}^*\ m_{z0}\ p_{z0}^*]^t \tag{18c}$$

The Lagrangian function can be re-stated with Eqs. (15), (16) and (18) as

$$L = \frac{1}{2}\int \dot{d}^t \bar{m} \dot{d}\, dx - \left\{\frac{1}{2}\int \bar{\varepsilon}^t \overline{D}\,\bar{\varepsilon}\, dx - d^t \int \underset{\sim}{P}\, dx\right\} \tag{19}$$

3. Finite element modeling

The displacements within an element can be expressed in terms of its nodal displacements in isoparametric formulations as

$$d = Nd_e \tag{20}$$

where N is the shape function vector [19] and d_e is a vector containing nodal displacement vectors of an element with $\boldsymbol{m}$ nodes and can be expressed as

$$d_e = \left[d_1^t\ d_2^t\ \cdots\ d_m^t\right]^t \tag{21}$$

Similarly, the strains with in an element can be written through Eqs. (5a) and (12b) as

$$\bar{\varepsilon} = \begin{bmatrix} B_a \\ B_b \\ B_t \\ B_s \end{bmatrix} d_e = \overline{B} d_e \tag{22}$$

where, for a given node m, the strain displacement matrix can be computed as

$$B_a = \begin{bmatrix} N_{,x} & N/R & 0 & 0 & 0 & 0 & 0 \\ 0 & 0 & 0 & N_{,x} & 0 & 0 & N/R \end{bmatrix}_m \tag{23}$$

$$B_b = \begin{bmatrix} 0 & 0 & N_{,x} & 0 & 0 & N/R & 0 \\ 0 & 0 & 0 & 0 & N/R & 0 & 0 \end{bmatrix}_m \tag{24}$$

$$B_t = \begin{bmatrix} 0 & 0 & 0 & 0 & 0 & N & 0 \\ 0 & 0 & 0 & 0 & 0 & 0 & 2N \end{bmatrix}_m \tag{25}$$

$$B_s = \begin{bmatrix} -N/R & N_{,x} & N & 0 & 0 & 0 & 0 \\ 0 & 0 & 0 & -N/R & 3N & 0 & N_{,x} \\ 0 & 0 & -N/R & 2N & 0 & N_{,x} & 0 \\ 0 & 0 & 0 & 0 & -N/R & 0 & 0 \end{bmatrix}_m \tag{26}$$

By substituting Eqs. (20) and (22) in Eq. (19), one gets,

$$L = \frac{1}{2}\dot{d}_e^t \int N^t \bar{m} N \, dx \dot{d}_e - \left\{ \frac{1}{2} d_e^t \int \bar{B}^t \bar{D} \bar{B} dx d_e - d_e^t \left[P_c + \int N^t \underset{\sim}{P} \, dx \right] \right\} \tag{27}$$

Applying Hamilton's principle on L, we get the governing equation of motion as

$$M\ddot{d} + Kd = F(t) \tag{28}$$

where

$$M = \int N^t \bar{m} N \, dx \tag{28a}$$

$$K = \int \bar{B}^t \bar{D} \bar{B} \, dx \tag{28b}$$

$$F(t) = \left(P_c + \int N^t \underset{\sim}{P} \, dx \right) p(t) \tag{28c}$$

The external force vector of Eq. (28c) can be expressed as

$$F(t) = \left(P_c + \sum w_g N^t \underset{\sim}{P} |J| \right) p(t) \tag{29}$$

Table 1
Temporal distribution of loading function.

Triangular pulse loading-1		
	$p(t) = t/t_p$	for $(0 \leqslant t \leqslant t_p)$
	$= 1 - [(t - t_p)/(t_f - t_p)]$	for $(t_p < t \leqslant t_f)$
	$= 0$	for $(t > t_f)$
Triangular pulse loading-2		
	$p(t) = 1 - t/t_f$	for $(0 \leqslant t \leqslant t_f)$
	$= 0$	for $(t > t_f)$
Step pulse loading		
	$p(t) = 1$	for $(0 \leqslant t \leqslant t_f)$
	$= 0$	for $(t > t_f)$
Sine pulse loading		
	$p(t) = \sin(\pi t/t_f)$	for $(0 \leqslant t \leqslant t_f)$
	$= 0$	for $(t > t_f)$
Blast (exponential) loading		
	$p(t) = e^{-\delta t}$	
Newmark method constants	$\gamma = 0.5$, $\beta = 0.25$	

Table 2
Boundary conditions for different supports.

Support type	At $x = 0$	At $x = S$
Simply supported (SS)	$u_0 = u_0^* = 0$	$u_0 = u_0^* = 0$
	$w_0 = \theta_z = w_0^* = 0$	$w_0 = \theta_z = w_0^* = 0$
Clamped–clamped (CC)	$u_0 = u_0^* = \theta_x = \theta_x^* = 0$	$u_0 = u_0^* = \theta_x = \theta_x^* = 0$
	$w_0 = \theta_z = w_0^* = 0$	$w_0 = \theta_z = w_0^* = 0$
Clamped–free (CF)	$u_0 = u_0^* = \theta_x = \theta_x^* = 0$	All free
	$w_0 = \theta_z = w_0^* = 0$	
Pinched ring (PR)	$u_0 = u_0^* = \theta_x = \theta_x^* = 0$	$u_0 = u_0^* = \theta_x = \theta_x^* = 0$

where

P_c – the vector of nodal concentrated loads of an element (29a)

$$\underset{\sim}{P} = b \left[0 \; p_z \; 0 \; 0 \; 0 \; \frac{t}{2} \; p_z \; \frac{t^2}{4} \; p_z \right] \tag{29b}$$

Table 3
Material data for validation experiments.

No	Details	Ref.
Data-3.1	Beam $E_1 = E_2 = E_3 = 1.2 \times 10^4$ lb/in.^{2} $G_{12} = G_{23} = G_{13} = 0.5 \times 10^4$ lb/in.^{2} $S = 10$ in., $b = 1$ in., $t = 1$ in. $v = 0.2$ $\rho = 1.0 \times 10^{-6}$ lb s^2/in.^{4} Load: $p_z = 2.85$ lb/in; step pulse loading – $t_f = 0.013$ s No. of elements: 8 cubic BC: CF	Bathe et al. [21]
Data-3.2	Beam $E_1 = E_2 = E_3 = 3.0 \times 10^7$ lb/in.^{2} $G_{12} = G_{23} = G_{13} = 1.4286 \times 10^7$ lb/in.^{2} $S = 20$ in., $b = 1$ in., $t = 0.125$ in. $v = 0.05$ $\rho = 2.5374 \times 10^{-4}$ lb s^2/in.^{4} Load: $p_c = 640$ lb; step pulse loading – $t_f = 0.005$ s No. of elements: 16 cubic BC: CC	Mondkar and Powell [22]
Data-3.3	Beam $E_1 = E_2 = E_3 = 3.0 \times 10^7$ lb/in.^{2} $G_{12} = G_{23} = G_{13} = 1.1538 \times 10^7$ lb/in.^{2} $S = 30$ in., $b = 1$ in., $t = 2$ in. $v = 0.3$ $\rho = 0.733 \times 10^{-3}$ lb s^2/in.^{4} Load: $p_z = 220$ lb/in.; step pulse loading – $t_f = 0.007$ s No. of elements: 16 cubic BC: SS	Liu and Lin [23]
Data-3.4	Circular arch $E_1 = E_2 = E_3 = 1.0 \times 10^7$ lb/in.^{2} $G_{12} = G_{23} = G_{13} = 4.1667 \times 10^6$ lb/in.^{2} $S = 210.848$ in., $R = 67.115$ in., $\beta = 180^o$ $b = 1$ in., $t = 1$ in. $v = 0.1999$ $\rho = 2.44 \times 10^{-4}$ lb s^2/in.^{4} Load1: $p_c = 700$ lb; step pulse loading – $t_f = 0.072$ s Load2: $p_c = 2100$ lb; triangular pulse loading-1 $t_p = 250$ μs; $t_f = 500$ μs No. of elements: 16 cubic BC: CC	Noor and Knight [8]
Data-3.5	Shallow arch $E_1 = 40 \times 10^6$ lb/in.^{2}, $E_2 = E_3 = 1.0 \times 10^6$ lb/in.^{2} $G_{12} = G_{13} = 0.6 \times 10^6$ lb/in.^{2}, $G_{23} = 0.5 \times 10^6$ lb/in.^{2} $S = 20$ in., $R = 100$ in., $\beta = 11.45916^o$ $b = 1$ in., $t = 2$ in. $v = 0.25$ $\rho = 1.2 \times 10^{-4}$ lb s^2/in.^{4} Load: sinusoidal load with central amplitude $p_z = 50$ lb/in.; Triangular pulse loading-2 with $t_f = 0.005$ s, Sine pulse loading with $t_f = 0.005$ s, Step pulse loading with $t_f = 0.005$ s, Blast loading with $\delta = 660$ s^{-1}, $t_f = 0.005$ s No. of elements: 8 cubic BC: CC Lamination – $[0/90]_6$ for sine pulse loading; for all others [0/90/0]	Khdeir and Reddy [12]

Table 4
Material data for HOAM experiments.

Material data – sandwich	
Face: Graphite/Epoxy	Chen and Sun [24] E_x = 120.11 GPa (0.1742×10^8 lb/in.^{2}) $E_y = E_z$ = 7.9083 GPa (0.1147×10^7 lb/in.^{2}) $G_{xy} = G_{yz} = G_{xz}$ = 5.5041 GPa (0.7983×10^6 lb/in.^{2}) $kG_{xy} = kG_{yz} = kG_{xz}$ = 4.5871 GPa (0.6653×10^6 lb/in.^{2}) $\rho_f = 0.1433 \times 10^{-3}$ lb s^2/in.^{4} v_f = 0.3
Core: Aluminium honeycomb (0.25 in cell size, 0.007 in foil)	Allen [25] $E_x = E_y = E_z = G_{xy} = v_c = 0$. G_{yz} = 70.395 MPa (0.1021×10^5 lb/in.^{2}) G_{xz} = 140.79 MPa (0.2042×10^5 lb/in.^{2}) kG_{yz} = 58.661 MPa (0.8508×10^4 lb/in.^{2}) kG_{xz} = 117.35 MPa (0.1702×10^5 lb/in.^{2}) $\rho_c = 0.3098 \times 10^{-5}$ lb s^2/in.^{4} t_c/t_f = 8
Material data – composite	Reddy[26] E_x = 525.38 GPa(0.762×10^8 lb/in.^{2}) $E_y = E_z$ = 21.015 GPa (0.3048×10^7 lb/in.^{2}) $G_{xy} = G_{yz} = G_{xz}$ = 10.508 GPa (0.1524×10^7 lb/in.^{2}) $kG_{xy} = kG_{yz} = kG_{xz}$ = 8.7563 GPa (0.127×10^7 lb/in.^{2}) $\rho = 0.72567 \times 10^{-4}$ lb s^2/in.^{4} v = 0.25
Data-4.1	Circular arch Material data – sandwich S = 7979.6 mm (314.1593 in.), R = 2540 mm (100 in.) β = 180° b = 25.4 mm (1 in.) Load: p_c = 444.82 N (100 lb); step pulse loading – t_f = 0.02 s No. of elements: 16 cubic BC: CC Lamination: [0/30/45/60/core/60/45/30/0] Aspect ratios: 5, 10, 15, and 25
Data-4.2	Pinched ring Material data – sandwich S (of quarter ring) = 197.62 mm (7.7802 in.) R = 125.81 mm (4.953 in.) β = 90° b = 25.4 mm (1 in.) Load: p_c = 444.82 N (100 lb); load on quarter ring = 222.41 N (50 lb); Step pulse loading – t_f = 0.025 s No. of elements: 8 cubic BC: PR Lamination: [0/90/core/0/90] Aspect ratios: 5, 10, 15, and 25
Data-4.3	Cantilever quarter arch Material data – composite S = 2677.7696 mm (105.424 in.), R = 1704.721 mm (67.115 in.) β = 90° b = 25.4 mm (1 in.) Load: p_c = 3336.15 N (750 lb); step pulse loading – t_f = 0.07 s No. of elements: 8 cubic BC: CF Lamination: [30/−30/30] Aspect ratios: 5, 10, 15, and 25
Data-4.4	Shallow arch Material data – composite S = 892.59156 mm (35.1414 in.), R = 1704.721 mm (67.115 in.) β = 30° b = 25.4 mm (1 in.) Load: p_z = 455 lb/in.; step pulse loading – t_f = 0.004 s No. of elements: 16 cubic BC: SS Lamination: [0/45/−45/90] Aspect ratios: 5, 10, 15, and 25

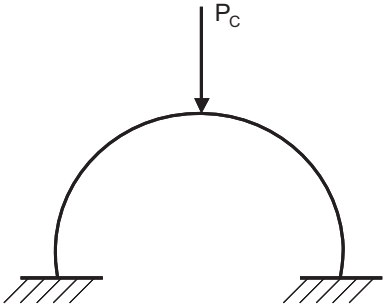

Fig. 2a. Circular arch with central load.

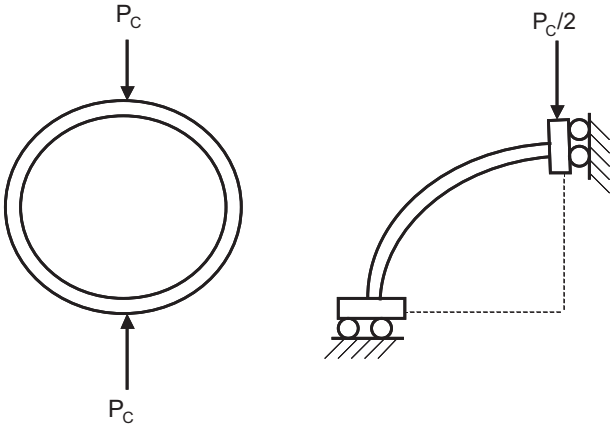

Fig. 2b. Pinched ring and its quarter model.

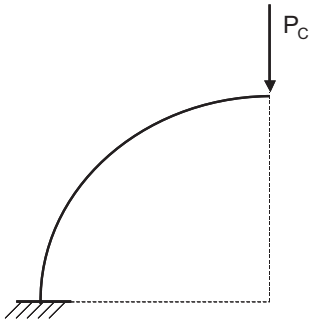

Fig. 2c. Quarter arch with tip load.

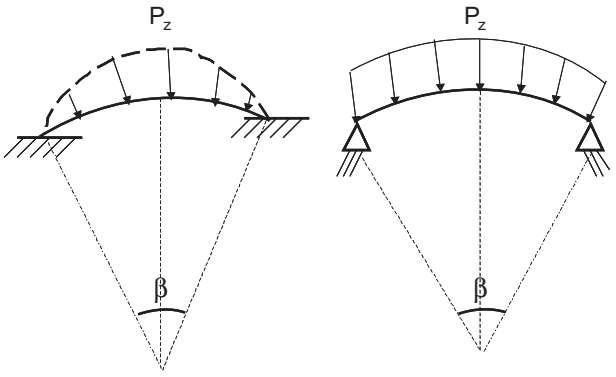

Fig. 2d. Shallow arch with sinusoidal and uniformly distributed load.

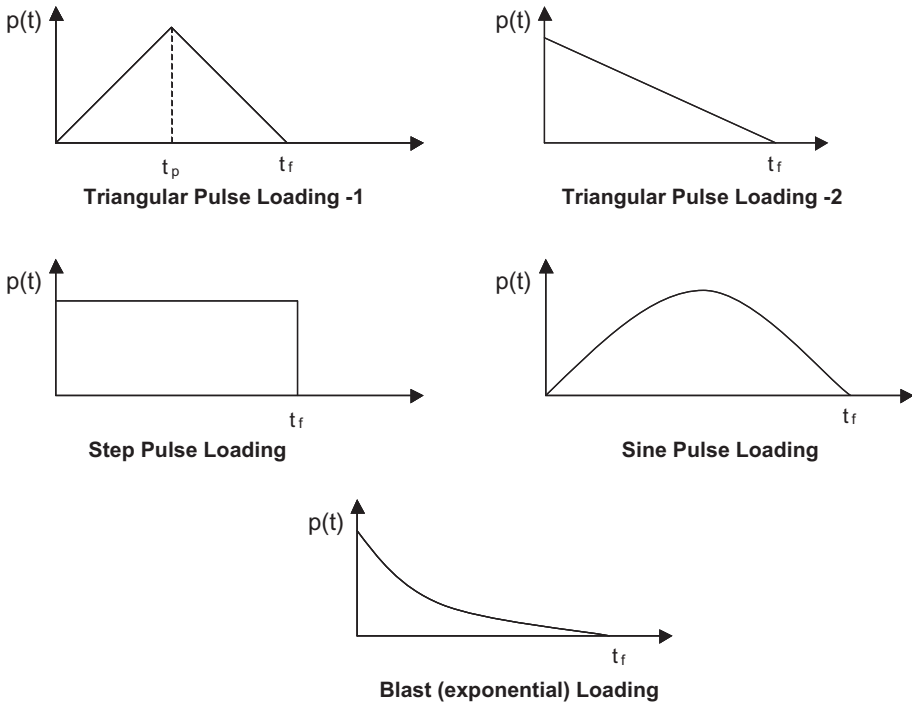

Fig. 3. Temporal variation of dynamic load.

p_z – uniformly distributed transverse load or (29c)

p_z – central amplitude of sinusoidal load (29d)

$p(t)$ – temporal variation of the forcing function as given in Table1 (29e)

4. Solution to equation of dynamic equilibrium

The equation of dynamic equilibrium Eq. (28) with damping can be expressed in an incremental form as

$$M\Delta a + C\Delta v + K\Delta d = \Delta F \tag{30}$$

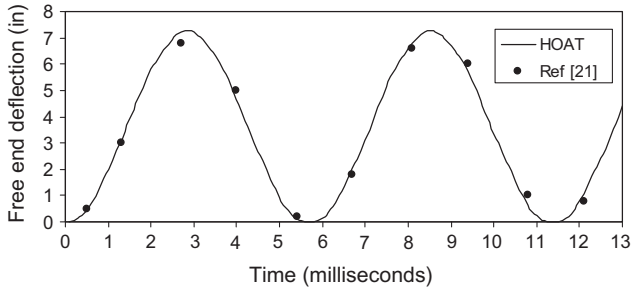

Fig. 4. Transient response of a cantilever beam (Data-3.1).

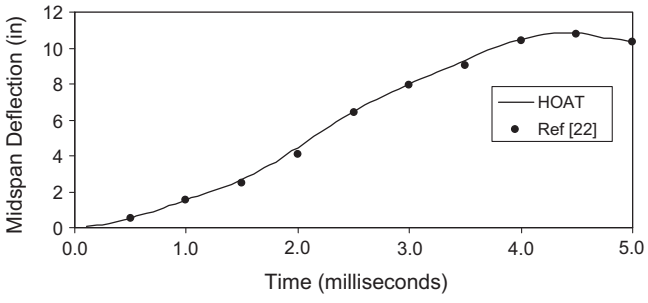

Fig. 5. Transient response of a clamped beam (Data-3.2).

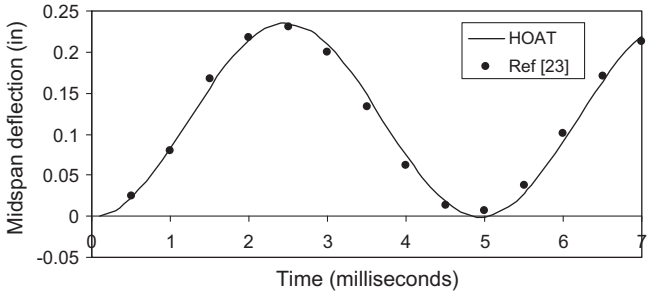

Fig. 6. Transient response of SS beam (Data-3.3).

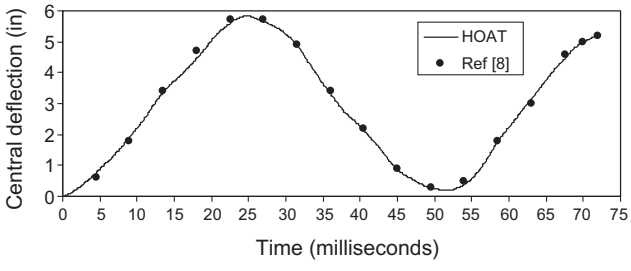

Fig. 7. Transient response of a clamped semi-circular arch with step loading (Data-3.4).

where

$$\Delta a = (a_{n+1} - a_n) = (\ddot{d}_{n+1} - \ddot{d}_n) \tag{30a}$$

$$\Delta v = (v_{n+1} - v_n) = (\dot{d}_{n+1} - \dot{d}_n) \tag{30b}$$

$$\Delta d = (d_{n+1} - d_n) \tag{30c}$$

$$\Delta F = (F_{n+1} - F_n) \tag{30d}$$

and the subscript $n+1$ and n represent quantities at time t_{n+1} and t_n respectively. The solution to this equation through Newmark Beta method [20] can be obtained as

$$v_{n+1} = v_n + (1-\gamma)a_n\Delta t + \gamma a_{n+1}\Delta t \tag{31}$$

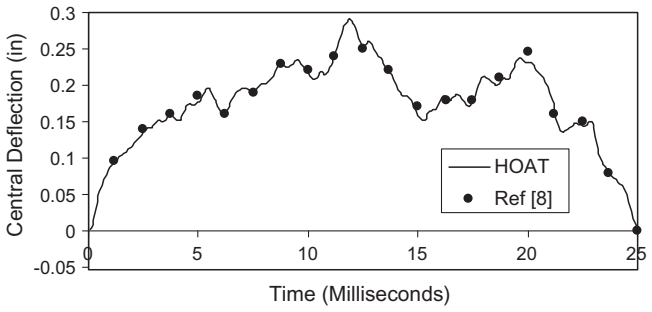

Fig. 8. Transient response of a clamped semi-circular arch with triangular loading (Data-3.4).

$$d_{n+1} = d_n + v_n\Delta t + \left(\frac{1}{2} - \beta\right)a_n\Delta t^2 + \beta a_{n+1}\Delta t^2 \tag{32}$$

where γ and β are the parameters adopted in Newmark's method and $\Delta t = t_{n+1} - t_n$.

Eqs. (31) and (32) can be expressed in incremental form as

$$\Delta v = (1-\gamma)a_n\Delta t + \gamma a_{n+1}\Delta t \tag{33}$$

$$\Delta d = v_n\Delta t + \left(\frac{1}{2} - \beta\right)a_n\Delta t^2 + \beta a_{n+1}\Delta t^2 \tag{34}$$

Substituting Eqs. (33), (34) and (30a) in Eq. (30), one gets

$$M\Delta a + C[(1-\gamma)a_n\Delta t + \gamma a_n\Delta t + \gamma\Delta a\Delta t] + K[v_n\Delta t + \left(\frac{1}{2} - \beta\right)a_n\Delta t^2 + \beta a_n\Delta t^2 + \beta\Delta a\Delta t^2] = \Delta F \tag{35}$$

which after rearranging terms becomes,

$$\overline{M}\Delta a = \Delta\overline{F} \tag{36}$$

where

$$\overline{M} = [M + C\gamma\Delta t + K\beta\Delta t^2] \tag{36a}$$

$$\Delta\overline{F} = \left[\Delta F - Ca_n\Delta t - \left(v_n\Delta t + a_n\frac{\Delta t^2}{2}\right)K\right] \tag{36b}$$

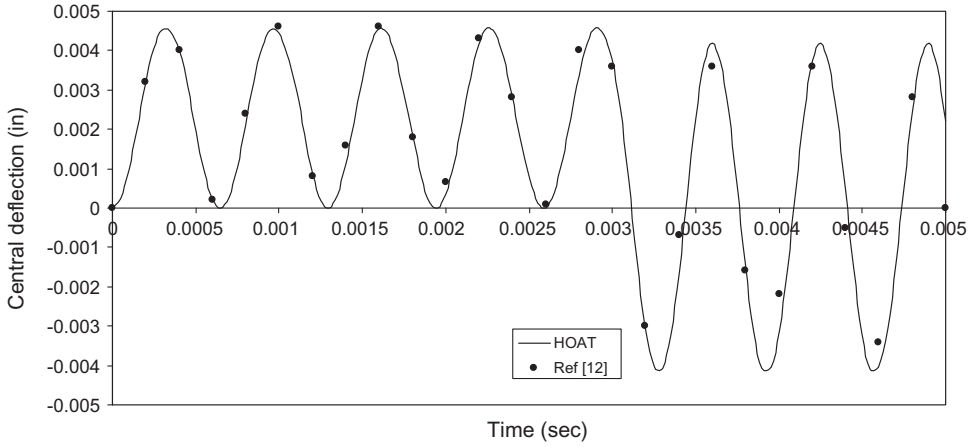

Fig. 9. Transient response of shallow arch to step pulse (Data-3.5).

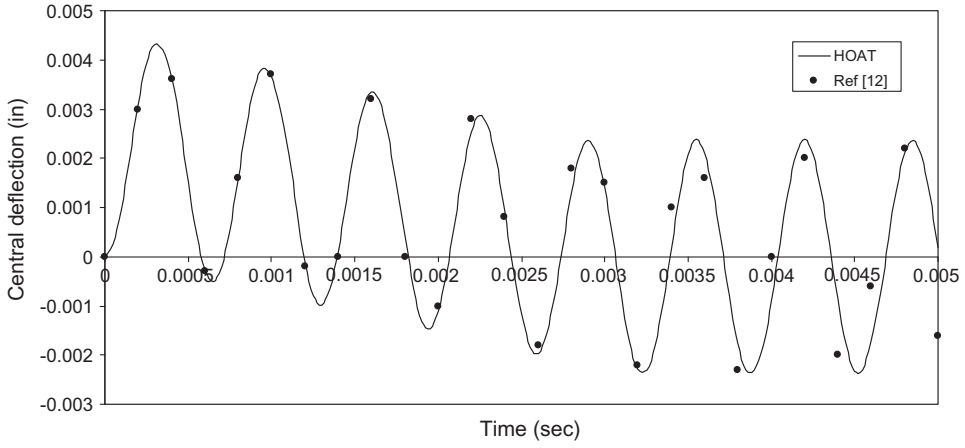

Fig. 10. Transient response of a shallow arch to triangular pulse (Data-3.5).

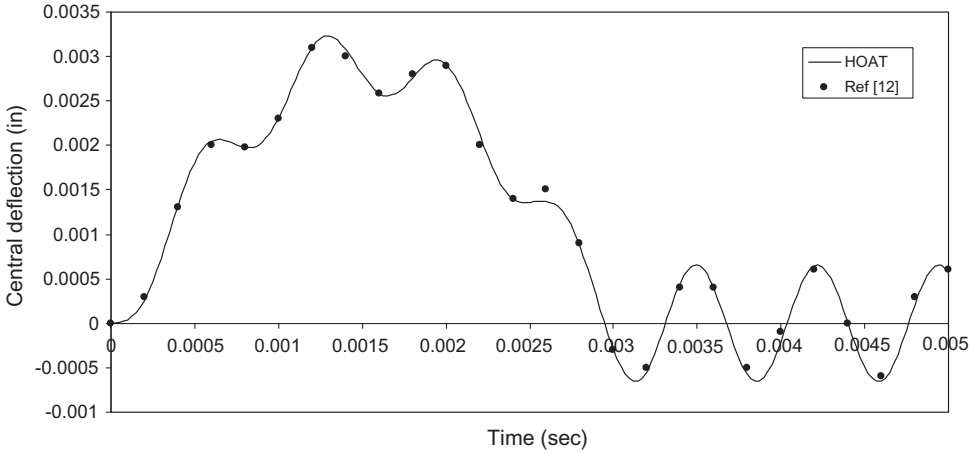

Fig. 11. Transient response of a shallow arch to sine pulse (Data-3.5).

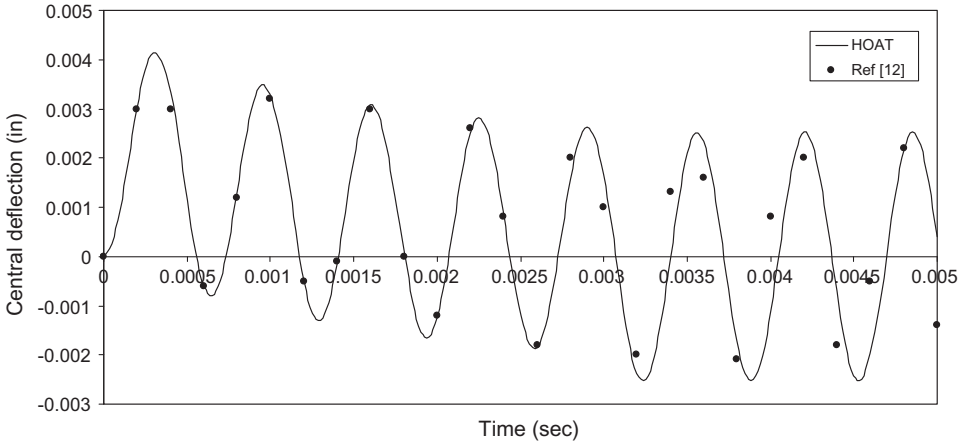

Fig. 12. Transient response of a shallow arch to blast loading (Data-3.5).

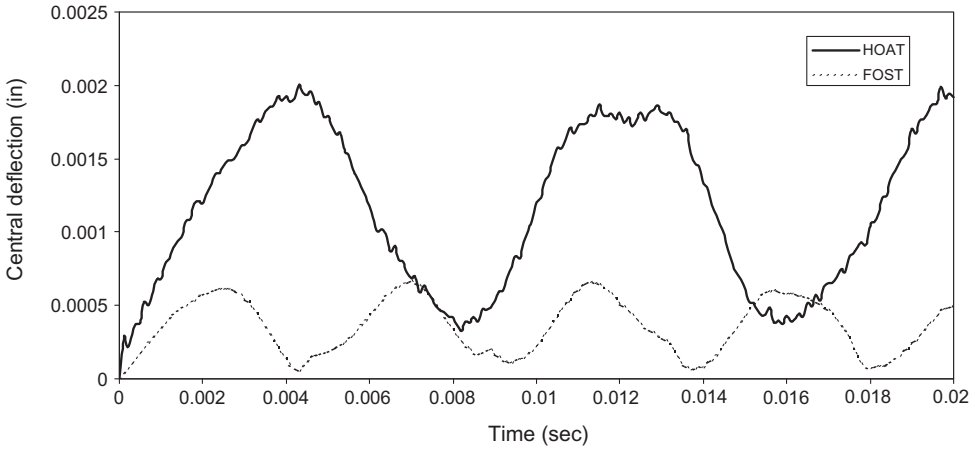

Fig. 13. Response of a circular arch – $S/t = 5$ (Data-4.1).

Here, Eq. (36) can be solved for Δa and current acceleration – a_{n+1}– can be computed using Eq. (30a). With the acceleration at current time step and Eqs. (33) and (34), Δv and Δd can be evaluated. The current velocity and displacement – v_{n+1} and d_{n+1} – can then be estimated from Eq. (30b) and (30c).

5. Numerical experiments

Numerical experiments have been carried out to study the performance of HOAM. This model is first validated through solving problems available in the literature and later its performance is

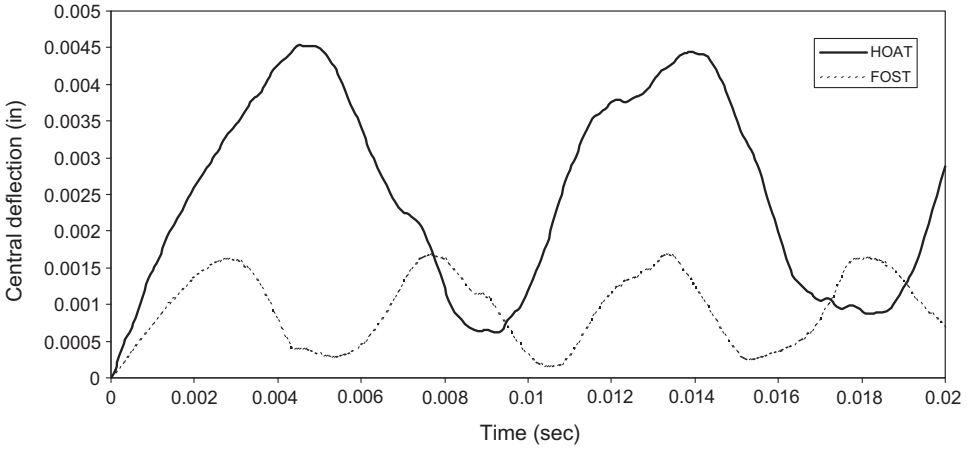

Fig. 14. Response of a circular arch – $S/t = 10$ (Data-4.1).

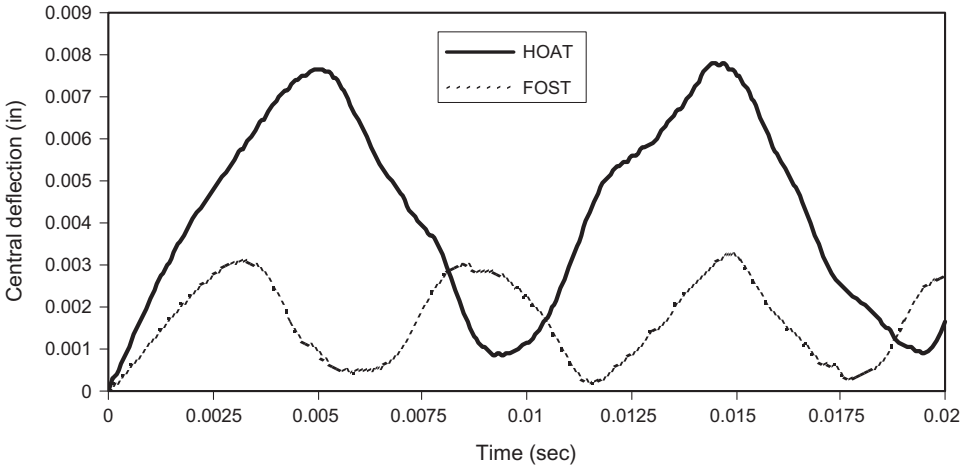

Fig. 15. Response of a circular arch – $S/t = 15$ (Data-4.1).

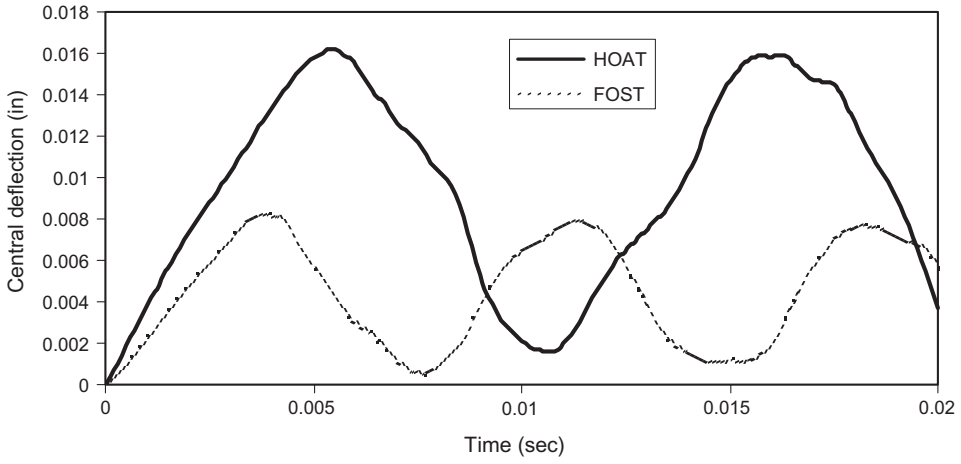

Fig. 16. Response of a circular arch – $S/t = 25$ (Data-4.1).

studied for various material and geometric conditions. For all the problems solved, various details such as material properties, lamination schemes, loading and end conditions are given in Tables 2–4 as well in Figs. 2 and 3.

5.1. Validation experiments

Few beam and arch problems are taken up first, in order to validate the proposed model.

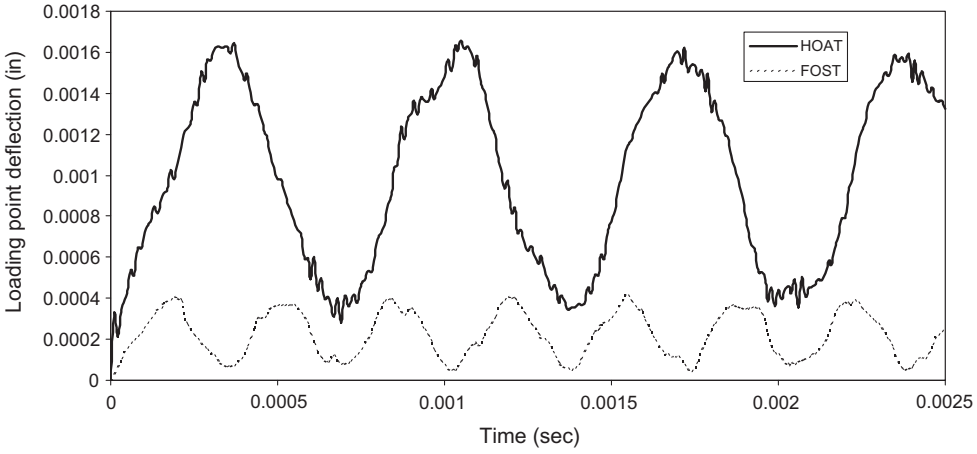

Fig. 17. Response of a pinched ring – $S/t = 5$ (Data-4.2).

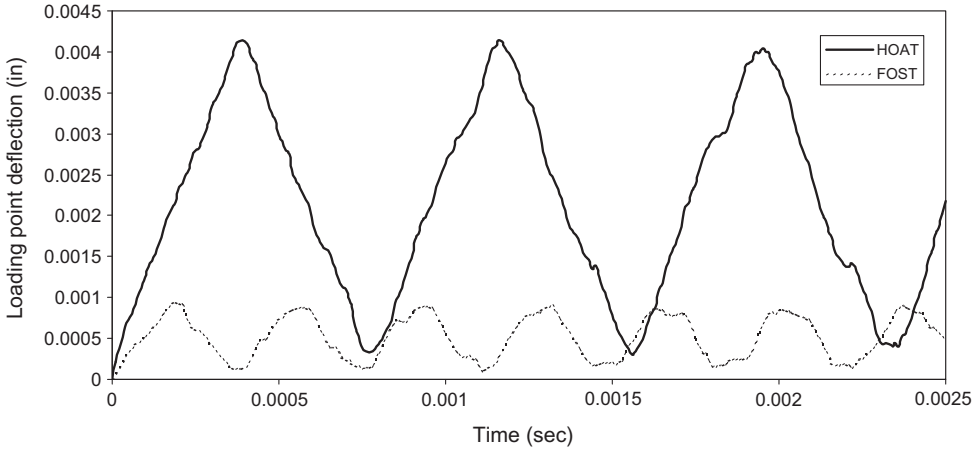

Fig. 18. Response of a pinched ring – $S/t = 10$ (Data-4.2).

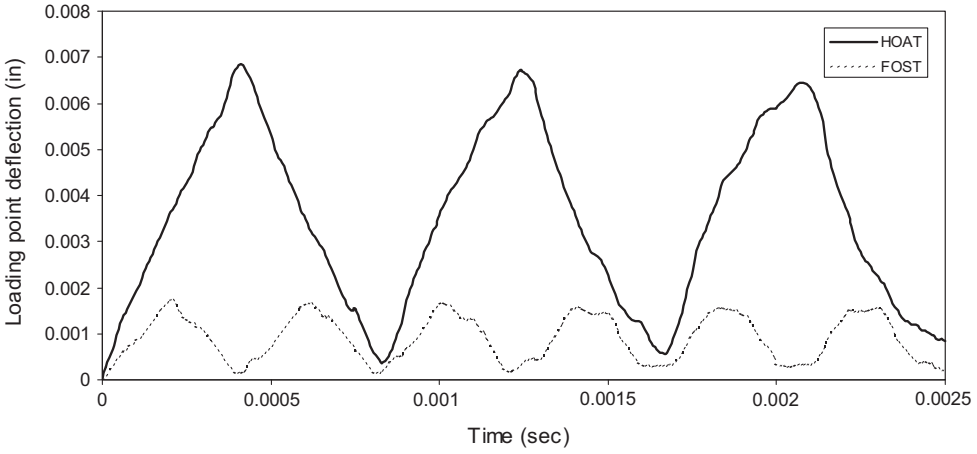

Fig. 19. Response of a pinched ring – $S/t = 15$ (Data-4.2).

A cantilever beam of Bathe et al. [21] subjected to uniformly distributed load, a clamped beam of Mondkar and Powell [22] with a central concentrated load and a simply supported beam of Liu and Lin [23] with uniformly distributed load are analyzed with HOAM and the results are presented in (Figs. 4–6). The close correlation between the earlier results and those of present model can be seen from these plots.

Next, a semi-circular arch of Noor and Knight [8] with a step pulse load and a triangular pulse loading is studied and the results of HOAT are presented in Figs. 7 and 8. Here also, close correlation

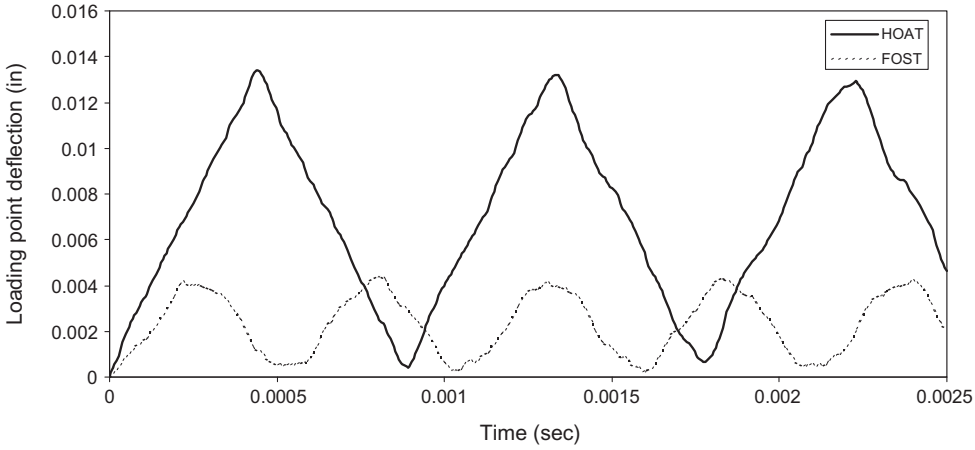

Fig. 20. Response of a pinched ring – $S/t = 25$ (Data-4.2).

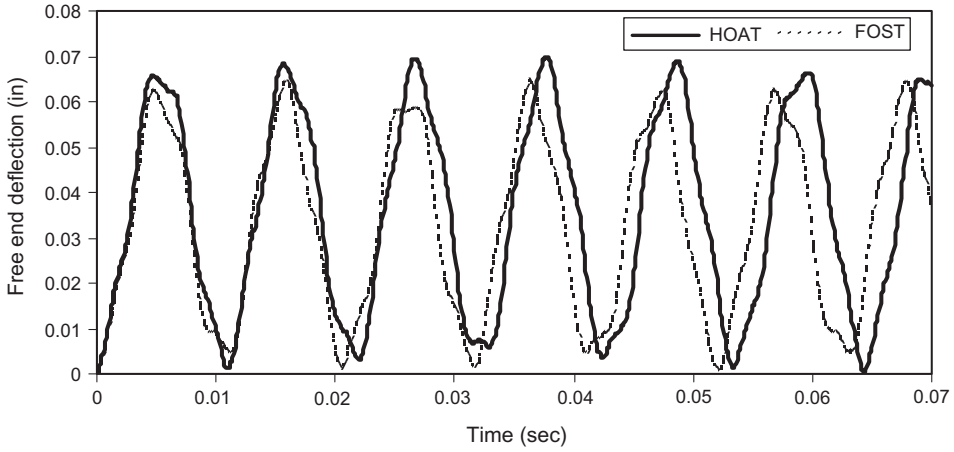

Fig. 21. Response of a quarter arch – $S/t = 5$ (Data-4.3).

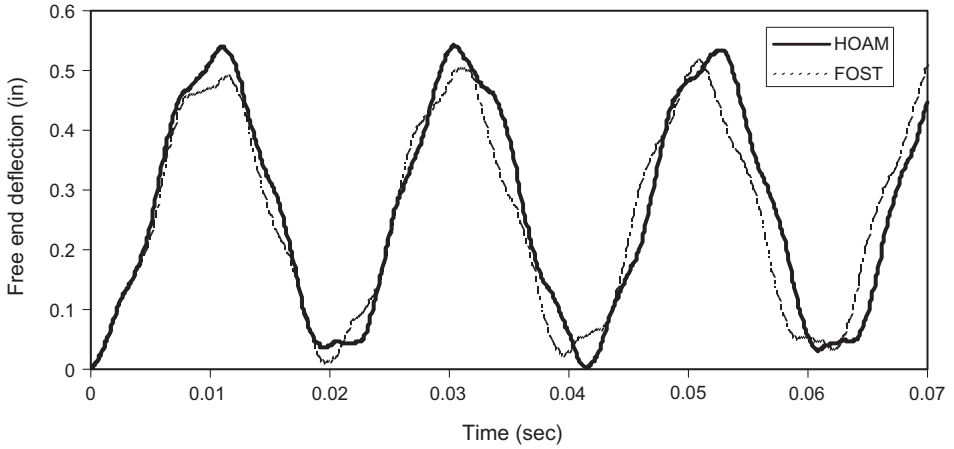

Fig. 22. Response of a quarter arch – $S/t = 10$ (Data-4.3).

between the current model and those of Noor and Knight can be observed.

A shallow cross-ply arch subjected to varieties of dynamic loadings, studied by Khdeir and Reddy [12] is analyzed by HOAM and its close correlation with the earlier results can be seen in Figs. 9–12.

Thus, with the correlations established with arches of varying curvature, aspect ratios, end conditions, material properties and transient dynamic loadings, the accuracy and adequacy of HOAM are validated in this section.

5.2. Higher order arch model (HOAM) experiments

A circular clamped arch with sandwich material and central concentrated load (Data-4.1) is analyzed with HOAM and first

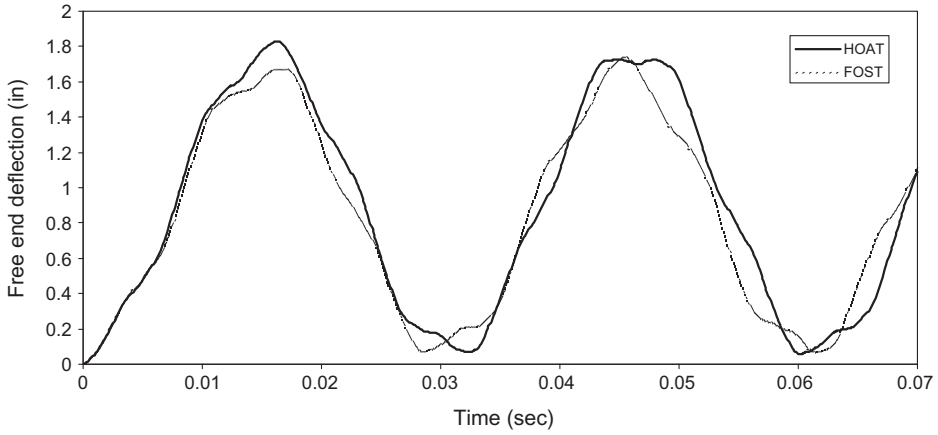

Fig. 23. Response of a quarter arch – $S/t = 15$ (Data-4.3).

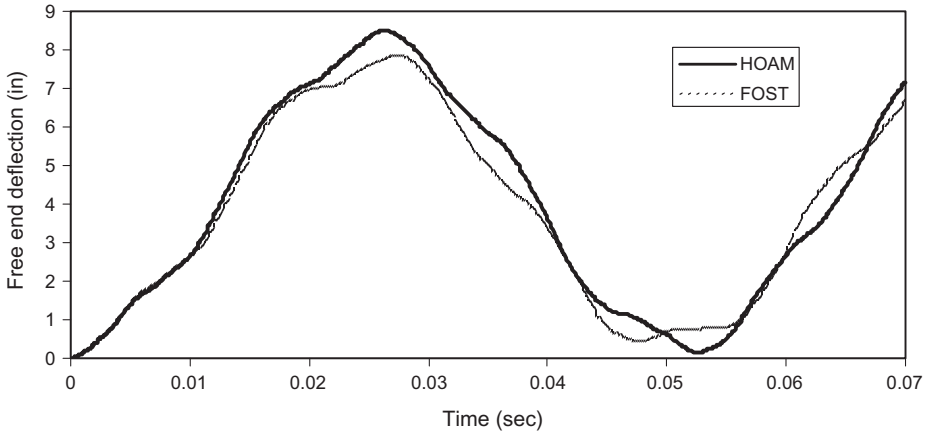

Fig. 24. Response of a quarter arch – $S/t = 25$ (Data-4.3).

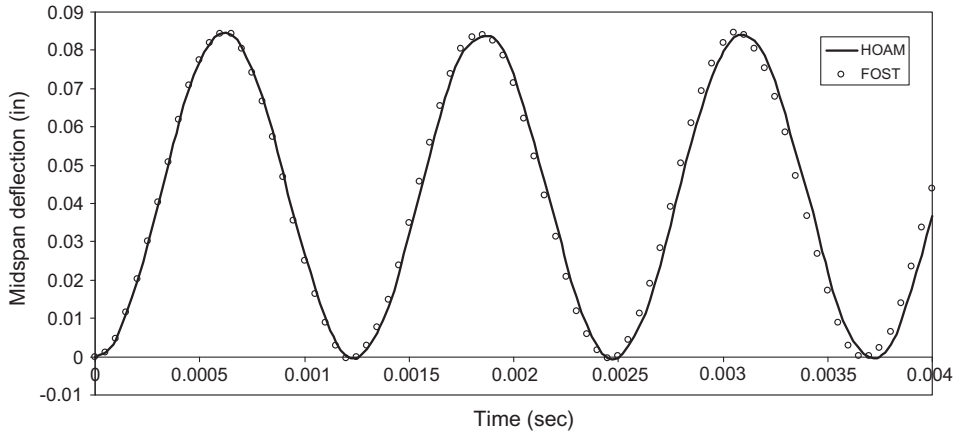

Fig. 25. Response of a shallow arch – $S/t = 5$ (Data-4.4).

order shear theory (FOST) for various aspect ratios of 5, 10, 15 and 25. The results are presented in Figs. 13–16.

In the case of thick arch of aspect ratio of five, it can be seen that deformations of HOAM are roughly four times than that of FOST and the period of the former is twice as much that of the latter. A similar significant order of difference, both for deformations as well as the period, can be observed for higher aspect ratios as well.

Next, a pinched ring with unsymmetric sandwich material (Data-4.2) is studied for various aspect ratios as shown in Figs. 17–20. In this case also, deformations of HOAM are almost four

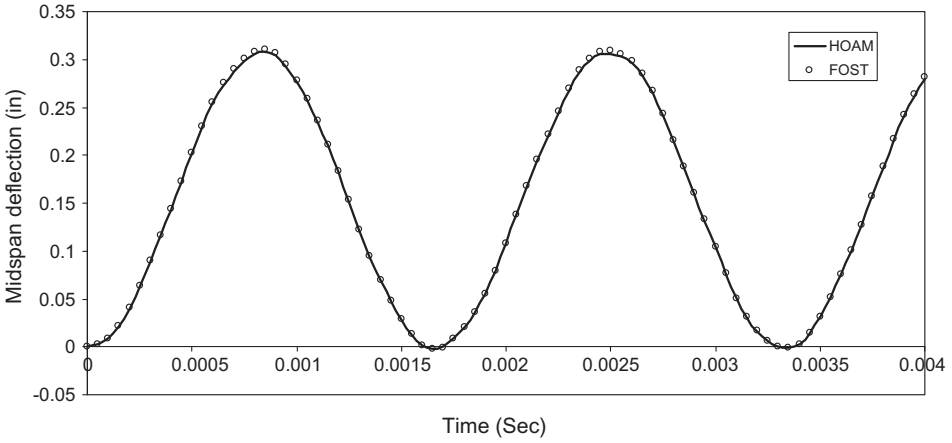

Fig. 26. Response of a shallow arch – $S/t = 10$ (Data-4.4).

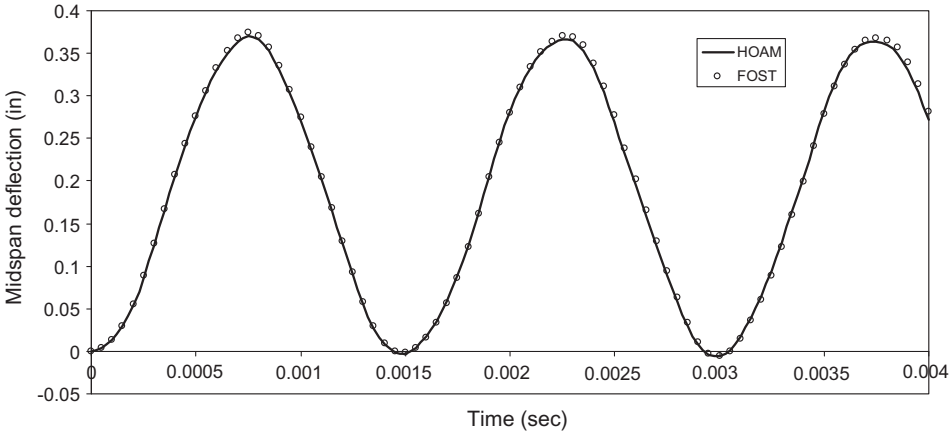

Fig. 27. Response of a shallow arch – $S/t = 15$ (Data-4.4).

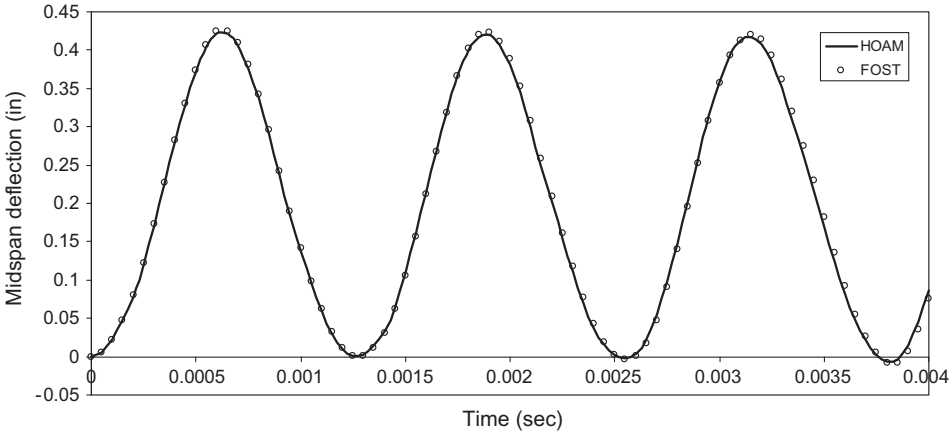

Fig. 28. Response of a shallow arch – $S/t = 5$ (Data-4.4).

times those of the FOST. The period of HOAM is twice than that of FOST, for all aspect ratios considered.

Composite structures are taken up next. A quarter arch with symmetric lamination (Data-4.3) with a tip load is analyzed for various aspect ratios as shown in Figs. 21–24. In this case, the deformations as well as the period of HOAM and FOST are quite close, with HOAM being slightly more flexible.

A composite shallow arch (Data-4.4) with uniformly distributed load is analyzed with the proposed model. The results for multiple aspect ratios are plotted in Figs. 25–28. It can be seen

that both HOAM and FOST predict identical results, from deep to thin arches.

6. Conclusions

A higher order model with isoparametric elements, which incorporates transverse shear and normal strain components, is presented in this paper for studying the transient dynamic response of laminated arches. The proposed model can study shallow to deep and thin to thick arch geometries with different end conditions and loadings quite effectively. Through the constitutive relationship, adapted from the three dimensional stress–strain relationship of an orthotropic lamina, even angle-ply laminates can be analyzed using one-dimensional elements. With the consistent mass matrix, governing equation of motion is solved through Newmark time marching scheme. The model is first validated with the available results in open literature and evaluated later for various arch geometries, laminations, and boundary as well as loading conditions and compared with the first order theory. It emerges from the numerical experiments that the proposed model is quite effective for deep sandwich constructions and performs as good as first order theory for laminated composite structures.

Appendix A

The stress–strain relationship at a point of an orthotropic lamina in a three-dimensional state of stress/strain can be expressed [17], along the lamina axes (Fig. 29) as

$$\sigma' = D\varepsilon' \tag{A1}$$

where

$$\sigma' = [\sigma_1\ \sigma_2\ \sigma_3\ \tau_{12}\ \tau_{23}\ \tau_{13}] \tag{A2}$$

$$\varepsilon' = [\varepsilon_1\ \varepsilon_2\ \varepsilon_3\ \gamma_{12}\ \gamma_{23}\ \gamma_{13}] \tag{A3}$$

$$D = \frac{1}{\Delta}\begin{bmatrix} E_1(1-\nu_{23}\nu_{32}) & E_1(\nu_{21}+\nu_{31}\nu_{23}) & E_1(\nu_{31}+\nu_{21}\nu_{32}) & 0 & 0 & 0 \\ E_2(\nu_{12}+\nu_{13}\nu_{32}) & E_2(1-\nu_{13}\nu_{31}) & E_2(\nu_{32}+\nu_{12}\nu_{31}) & 0 & 0 & 0 \\ E_3(\nu_{13}+\nu_{12}\nu_{23}) & E_3(\nu_{23}+\nu_{21}\nu_{13}) & E_3(1-\nu_{12}\nu_{21}) & 0 & 0 & 0 \\ 0 & 0 & 0 & \Delta G_{12} & 0 & 0 \\ 0 & 0 & 0 & 0 & \Delta G_{23} & 0 \\ 0 & 0 & 0 & 0 & 0 & \Delta G_{13} \end{bmatrix} \tag{A4}$$

$$\Delta = (1-\nu_{12}\nu_{21}-\nu_{23}\nu_{32}-\nu_{31}\nu_{13}-2\nu_{12}\nu_{23}\nu_{31}) \tag{A5}$$

The relation between engineering and tensor strain vectors, along lamina and laminate axes, can be given as

$$\varepsilon' = R\varepsilon'_{ts} \tag{A6}$$

$$\varepsilon^\circ = R\varepsilon^\circ_{ts} \tag{A7}$$

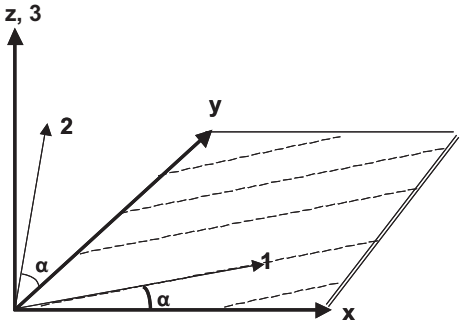

Fig. 29. Axis system – 1–3: Lamina axes; *x*, *y*, *z*: laminate axes.

where

$$R = \begin{bmatrix} 1 & 0 & 0 & 0 & 0 & 0 \\ 0 & 1 & 0 & 0 & 0 & 0 \\ 0 & 0 & 1 & 0 & 0 & 0 \\ 0 & 0 & 0 & 2 & 0 & 0 \\ 0 & 0 & 0 & 0 & 2 & 0 \\ 0 & 0 & 0 & 0 & 0 & 2 \end{bmatrix} \tag{A8}$$

If the angle between lamina and laminate axes can be defined as α, then the lamina to laminate axis transformation is given by,

$$T = \begin{bmatrix} c^2 & s^2 & 0 & 2sc & 0 & 0 \\ s^2 & c^2 & 0 & -2sc & 0 & 0 \\ 0 & 0 & 1 & 0 & 0 & 0 \\ -sc & sc & 0 & (c^2-s^2) & 0 & 0 \\ 0 & 0 & 0 & 0 & c & -s \\ 0 & 0 & 0 & 0 & s & c \end{bmatrix} \tag{A9}$$

where

$$\begin{aligned} c &= \cos\alpha \\ s &= \sin\alpha \end{aligned} \tag{A10}$$

and the stress and strain along the lamina and laminate axes can be equated as

$$\sigma' = T\sigma^\circ \tag{A11}$$

$$\varepsilon'_{ts} = T\varepsilon^\circ_{ts} \tag{A12}$$

By making use of Eqs. (A6)–(A12), one can get the laminate stress–strain relationship as

$$\sigma^\circ = Q\varepsilon^\circ \tag{A13}$$

where

$$Q = T^{-1}D(T^{-1})^t \tag{A14}$$

$$(T^{-1})^t = RTR^{-1} \tag{A15}$$

$$Q = \begin{bmatrix} Q_{11} & Q_{12} & Q_{13} & Q_{14} & 0 & 0 \\ Q_{21} & Q_{22} & Q_{23} & Q_{24} & 0 & 0 \\ Q_{31} & Q_{32} & Q_{33} & Q_{34} & 0 & 0 \\ Q_{41} & Q_{42} & Q_{43} & Q_{44} & 0 & 0 \\ 0 & 0 & 0 & 0 & Q_{55} & Q_{56} \\ 0 & 0 & 0 & 0 & Q_{65} & Q_{66} \end{bmatrix} \tag{A16}$$

$$Q_{11} = D_{11}c^4 + 2(D_{12}+2D_{44})s^2c^2 + D_{22}s^4 \tag{A17}$$

$$Q_{12} = D_{12}(s^4+c^4) + (D_{11}+D_{22}-4D_{44})s^2c^2 \tag{A18}$$

$$Q_{13} = D_{31}c^2 + D_{32}s^2 \tag{A19}$$

$$Q_{14} = (D_{11}-D_{12}-2D_{44})sc^3 + (D_{12}-D_{22}+2D_{44})s^3c \tag{A20}$$

$$Q_{22} = D_{11}s^4 + 2(D_{12}+2D_{44})s^2c^2 + D_{22}c^4 \tag{A21}$$

$$Q_{23} = D_{13}s^2 + D_{23}c^2 \tag{A22}$$

$$Q_{24} = (D_{11}-D_{12}-2D_{44})s^3c + (D_{12}-D_{22}+2D_{44})sc^3 \tag{A23}$$

$$Q_{33} = D_{33} \tag{A24}$$
$$Q_{34} = (D_{13} - D_{23})sc \tag{A25}$$
$$Q_{44} = (D_{11} - 2D_{12} + D_{22} - 2D_{44})s^2c^2 + D_{44}(c^4 + s^4) \tag{A26}$$
$$Q_{55} = D_{55}c^2 + D_{66}s^2 \tag{A27}$$
$$Q_{56} = (D_{66} - D_{55})sc \tag{A28}$$
$$Q_{66} = D_{55}s^2 + D_{66}c^2 \tag{A29}$$

Appendix B

$$\Phi = (Q_{22}Q_{44} - Q_{24}^2) \tag{B1}$$
$$C_{11} = Q_{11} + \frac{Q_{12}}{\Phi}(Q_{14}Q_{24} - Q_{12}Q_{44}) + \frac{Q_{14}}{\Phi}(Q_{12}Q_{24} - Q_{14}Q_{22}) \tag{B2}$$
$$C_{12} = Q_{13} + \frac{Q_{12}}{\Phi}(Q_{24}Q_{34} - Q_{23}Q_{44}) + \frac{Q_{14}}{\Phi}(Q_{23}Q_{24} - Q_{22}Q_{34}) \tag{B3}$$
$$C_{21} = Q_{13} + \frac{Q_{23}}{\Phi}(Q_{14}Q_{24} - Q_{12}Q_{44}) + \frac{Q_{34}}{\Phi}(Q_{12}Q_{24} - Q_{14}Q_{22}) \tag{B4}$$
$$C_{22} = Q_{33} + \frac{Q_{23}}{\Phi}(Q_{24}Q_{34} - Q_{23}Q_{44}) + \frac{Q_{34}}{\Phi}(Q_{23}Q_{24} - Q_{22}Q_{34}) \tag{B5}$$
$$C_{33} = Q_{66} - \frac{Q_{56}^2}{Q_{55}} \tag{B6}$$

Appendix C

Using binomial series, the following terms can be expanded as

$$\frac{1}{(1+z/R)} = 1 - \frac{z}{R} + \frac{z^2}{R^2} - \frac{z^3}{R^3} \tag{C1}$$
$$\frac{1}{(1+z/R)^2} = 1 - \frac{2z}{R} + \frac{3z^2}{R^2} - \frac{4z^3}{R^3} \tag{C2}$$

which are used in the evaluation of various D matrices.

$$D_{aa} = b\int Z_a C_{11} Z_a^t dz = b\sum_{l=1}^{NL} C_{11}\begin{bmatrix} H_1 - \frac{2}{R}H_2 + \frac{3}{R^2}H_3 - \frac{4}{R^3}H_4 & H_3 - \frac{2}{R}H_4 + \frac{3}{R^2}H_5 - \frac{4}{R^3}H_6 \\ H_3 - \frac{2}{R}H_4 + \frac{3}{R^2}H_5 - \frac{4}{R^3}H_6 & H_5 - \frac{2}{R}H_6 + \frac{3}{R^2}H_7 - \frac{4}{R^3}H_8 \end{bmatrix} \tag{C3}$$

$$D_{ab} = b\int Z_a C_{11} Z_b^t dz = b\sum_{l=1}^{NL} C_{11}\begin{bmatrix} H_2 - \frac{2}{R}H_3 + \frac{3}{R^2}H_4 - \frac{4}{R^3}H_5 & H_4 - \frac{2}{R}H_5 + \frac{3}{R^2}H_6 - \frac{4}{R^3}H_7 \\ H_4 - \frac{2}{R}H_5 + \frac{3}{R^2}H_6 - \frac{4}{R^3}H_7 & H_6 - \frac{2}{R}H_7 + \frac{3}{R^2}H_8 - \frac{4}{R^3}H_9 \end{bmatrix} \tag{C4}$$

$$D_{ba} = D_{ab}$$

$$D_{bb} = b\int Z_b C_{11} Z_b^t dz = b\sum_{l=1}^{NL} C_{11}\begin{bmatrix} H_3 - \frac{2}{R}H_4 + \frac{3}{R^2}H_5 - \frac{4}{R^3}H_6 & H_5 - \frac{2}{R}H_6 + \frac{3}{R^2}H_7 - \frac{4}{R^3}H_8 \\ H_5 - \frac{2}{R}H_6 + \frac{3}{R^2}H_7 - \frac{4}{R^3}H_8 & H_7 - \frac{2}{R}H_8 + \frac{3}{R^2}H_9 - \frac{4}{R^3}H_{10} \end{bmatrix} \tag{C5}$$

$$D_{at} = b\int Z_a C_{12} Z_t^t dz = b\sum_{l=1}^{NL} C_{12}\begin{bmatrix} H_1 - \frac{2}{R}H_2 + \frac{3}{R^2}H_3 - \frac{4}{R^3}H_4 & H_2 - \frac{2}{R}H_3 + \frac{3}{R^2}H_4 - \frac{4}{R^3}H_5 \\ H_3 - \frac{2}{R}H_4 + \frac{3}{R^2}H_5 - \frac{4}{R^3}H_6 & H_4 - \frac{2}{R}H_5 + \frac{3}{R^2}H_6 - \frac{4}{R^3}H_7 \end{bmatrix} \tag{C6}$$

$$D_{bt} = b\int Z_b C_{12} Z_t^t dz = b\sum_{l=1}^{NL} C_{12}\begin{bmatrix} H_2 - \frac{2}{R}H_3 + \frac{3}{R^2}H_4 - \frac{4}{R^3}H_5 & H_3 - \frac{2}{R}H_4 + \frac{3}{R^2}H_5 - \frac{4}{R^3}H_6 \\ H_4 - \frac{2}{R}H_5 + \frac{3}{R^2}H_6 - \frac{4}{R^3}H_7 & H_5 - \frac{2}{R}H_6 + \frac{3}{R^2}H_7 - \frac{4}{R^3}H_8 \end{bmatrix} \tag{C7}$$

$$D_{ta} = b\int Z_t C_{21} Z_a^t dz = b\sum_{l=1}^{NL} C_{21}\begin{bmatrix} H_1 - \frac{2}{R}H_2 + \frac{3}{R^2}H_3 - \frac{4}{R^3}H_4 & H_3 - \frac{2}{R}H_4 + \frac{3}{R^2}H_5 - \frac{4}{R^3}H_6 \\ H_2 - \frac{2}{R}H_3 + \frac{3}{R^2}H_4 - \frac{4}{R^3}H_5 & H_4 - \frac{2}{R}H_5 + \frac{3}{R^2}H_6 - \frac{4}{R^3}H_7 \end{bmatrix} \tag{C8}$$

$$D_{tb} = b\int Z_t C_{21} Z_b^t dz = b\sum_{l=1}^{NL} C_{21}\begin{bmatrix} H_2 - \frac{2}{R}H_3 + \frac{3}{R^2}H_4 - \frac{4}{R^3}H_5 & H_4 - \frac{2}{R}H_5 + \frac{3}{R^2}H_6 - \frac{4}{R^3}H_7 \\ H_3 - \frac{2}{R}H_4 + \frac{3}{R^2}H_5 - \frac{4}{R^3}H_6 & H_5 - \frac{2}{R}H_6 + \frac{3}{R^2}H_7 - \frac{4}{R^3}H_8 \end{bmatrix} \tag{C9}$$

$$D_{tt} = b\int Z_t C_{22} Z_t^t dz = b\sum_{l=1}^{NL} C_{22}\begin{bmatrix} H_1 & H_2 \\ H_2 & H_3 \end{bmatrix} \tag{C10}$$

$$D_{ss} = b\int Z_s C_{33} Z_s^t dz = b\sum_{l=1}^{NL} C_{33}\begin{bmatrix} H_1 & H_3 & H_2 & H_4 \\ & H_5 & H_4 & H_6 \\ & & H_3 & H_5 \\ & sym & & H_7 \end{bmatrix} \tag{C11}$$

$$\bar{m} = b\sum_{l=1}^{NL} \rho_l \begin{bmatrix} H_1 & 0 & H_2 & H_3 & H_4 & 0 & 0 \\ & H_1 & 0 & 0 & 0 & H_2 & H_3 \\ & & H_3 & H_4 & H_5 & 0 & 0 \\ & & & H_5 & H_6 & 0 & 0 \\ & & & & H_7 & 0 & 0 \\ & & & & & H_3 & H_4 \\ & sym & & & & & H_5 \end{bmatrix} \tag{C12}$$

In Eqs. (C3)–(C12), for a given layer l,

$$H_k = \frac{1}{k}\left(h_l^k - h_{l-1}^k\right) \tag{C13}$$

where

NL = total number of layers of a cross-section
k = constant varying from 1 to 10
h_l = distance from the neutral axis to the top of a layer, l
h_{l-1} = distance from the neutral axis to the top of layer l-1 or bottom of layer l

References

[1] Wu RWH, Witmer EA. Finite-element analysis of large elastic–plastic transient deformations of simple structures. Am Inst Aeronaut Astronaut J 1971;9(9):1719–24.
[2] Wu RWH, Witmer EA. Nonlinear transient responses of structures by the spatial finite-element method. Am Inst Aeronaut Astronaut J 1973;11(8):1110–7.
[3] Timoshenko SP. On the correction for shear in differential equation for transverse vibrations of prismatic bars. Philos Mag 1921;41(6):744–6.
[4] Tene Y, Epstein M, Sheinman I. Dynamics of curved beams involving shear deformation. Int J Solids Struct 1975;11(7–8):827–40.
[5] Sagartz MJ. Transient response of three layered rings. ASME J Appl Mech 1977;44:299–304.
[6] Remseth SN. Nonlinear static and dynamic analysis of framed structures. J Comput Struct 1979;10(6):879–97.
[7] Sheinman I. Dynamic large-displacement analysis of curved beams involving shear deformation. Int J Solids Struct 1980;16(11):1037–49.
[8] Noor AK, Knight Jr NF. Nonlinear dynamic analysis of curved beams. Comput Methods Appl Mech Eng 1980;23:225–51.
[9] Noor AK, Peters JM. Penalty finite element models for nonlinear dynamic analysis. Am Inst Aeronaut Astronaut J 1986;24(2):312–20.
[10] Henrych J. The dynamics of arches. Amsterdam: Elsevier; 1981.
[11] Hsiao KM, Hsiao RT. A co-rotational formulation for nonlinear dynamic analysis of curved Euler beam. Comput Struct 1995;54(6):1091–7.
[12] Khdeir AA, Reddy JN. Free and forced vibration of cross-ply laminated composite shallow arches. Int J Solids Struct 1997;34(10):1217–34.
[13] Huang CS, Tseng YP, Lin CJ. In-plane transient responses of arch with variable curvature using dynamic stiffness method. ASCE J Eng Mech 1998;124(8):826–35.

[14] Gordon RW, Hollkamp JJ. Reduced-order modeling of the random response of curved beams using implicit condensation. AIAA 2006-1926, 47th AIAA/ASME/ASCE/AHS/ASC structures, structural dynamics, and materials conference, Newport, Rhode Island; 2006.
[15] Lo KH, Christensen RM, Wu EM. A higher order theory of plate deformation – part 1: homogeneous plates. ASME J Appl Mech 1977;44:663–8.
[16] Qatu MS. Vibration of laminated shells and plates. Oxford: Elsevier; 2004.
[17] Jones RM. Mechanics of composite materials. Tokyo: McGraw Hill Kogakusha; 1975.
[18] Vinayak RU, Prathap G, Naganarayana BP. Beam elements based on a higher order theory – I. Formulation and analysis of performance. Comput Struct 1996;58:775–89.
[19] Reddy JN. An introduction to the finite element method. McGraw Hill Higher Education; 2006.
[20] Newmark NM. A method of computation for structural dynamics. J Eng Mech Div, Am Soc Civil Eng 1959;85(7):67–94.
[21] Bathe KJ, Ramm E, Wilson E. Finite element formulations for large deformation dynamics analysis. Int J Numer Methods Eng 1975;9:353–86.
[22] Mondkar DP, Powell GH. Finite element analysis of non-linear static and dynamic response. Int J Numer Methods Eng 1977;11:499–520.
[23] Liu SC, Lin TH. Elastic-plastic dynamic analysis of structures using known elastic solutions. Earthq Eng Struct Dynam 1979;7:147–59.
[24] Chen JK, Sun CT. Nonlinear transient responses of initially stressed composite plates. Comput Struct 1985;21(3):513–20.
[25] Allen HG. Analysis and design of structural sandwich panels. London: Pergamon Press; 1969.
[26] Reddy JN. On the solutions to forced motions of rectangular composite plates. ASME J Appl Mech 1982;49(3):403–8.